

From Pixels to Gigapixels: Bridging Local Inductive Bias and Long-Range Dependencies with Pixel-Mamba

Zhongwei Qiu^{1,2,5,*}, Hanqing Chao^{1,2,6,*}, Tiancheng Lin^{1,2,6,*}, Wanxing Chang^{1,2},
Zijiang Yang^{1,7}, Wenpei Jiao^{1,8}, Yixuan Shen³, Yunshuo Zhang⁴, Yelin Yang⁴,
Wenbin Liu³, Hui Jiang⁴, Yun Bian³, Ke Yan^{1,2}, Dakai Jin¹, Le Lu¹

¹DAMO Academy, Alibaba Group, ²Hupan Lab

³Department of Radiology, Changhai Hospital, ⁴Department of Pathology, Changhai Hospital

⁵Zhejiang University, ⁶Fudan University, ⁷University of Science and Technology Beijing, ⁸Peking University

{qiuzhongwei.qzw, hanqing.chq}@alibaba-inc.com

Abstract

Histopathology plays a critical role in medical diagnostics, with whole slide images (WSIs) offering valuable insights that directly influence clinical decision-making. However, the large size and complexity of WSIs may pose significant challenges for deep learning models, in both computational efficiency and effective representation learning. In this work, we introduce Pixel-Mamba, a novel deep learning architecture designed to efficiently handle gigapixel WSIs. Pixel-Mamba leverages the Mamba module, a state-space model (SSM) with linear memory complexity, and incorporates local inductive biases through progressively expanding tokens, akin to convolutional neural networks. This enables Pixel-Mamba to hierarchically combine both local and global information while efficiently addressing computational challenges. Remarkably, Pixel-Mamba achieves or even surpasses the quantitative performance of state-of-the-art (SOTA) foundation models that were pretrained on millions of WSIs or WSI-text pairs, in a range of tumor staging and survival analysis tasks, **even without requiring any pathology-specific pretraining**. Extensive experiments demonstrate the efficacy of Pixel-Mamba as a powerful and efficient framework for end-to-end WSI analysis.

1. Introduction

Histopathology plays a pivotal role in medical diagnostics, serving as the gold standard for diagnosing and characterizing a wide range of diseases [7, 35]. By examining tissue microstructures, pathologists obtain critical insights into the nature and severity of conditions, which directly influence

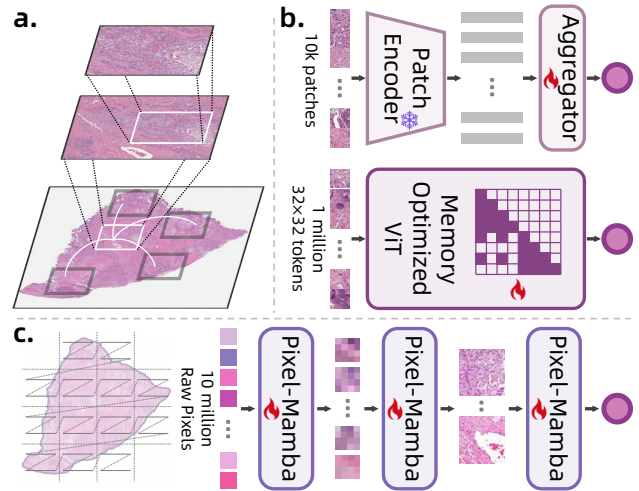


Figure 1. (a) Pathologists integrate observations from multiple regions across different scales to make a comprehensive assessment. (b) Frameworks of mainstream WSI analysis methods: a two-stage pipeline (top) and memory-optimized ViT (bottom, often with heavily pruned attention). (c) The proposed Pixel-Mamba, an end-to-end framework that combines progressive token expansion and the Mamba module to effectively integrate local inductive biases with long-range dependencies in a hierarchical manner.

treatment decisions and patient management [7, 35]. With the advent of WSI, computational pathology, driven by artificial intelligence (AI), has shown promise in addressing many challenges in Pathology, such as survival prediction, cancer subtyping, and predicting molecular alterations [20]. However, the large size of WSIs, which can reach up to $50,000 \times 50,000$ pixels, presents significant computational and methodological challenges for AI models.

From a computational perspective, even at low magnification, a single WSI can contain tens of millions of pixels,

*Equal Contribution

making training of deep learning models impractical. From a representation learning standpoint, WSIs introduce two key challenges: 1) balancing local information with long-range dependencies and 2) managing hierarchical structures across multiple scales. For example, tertiary lymphoid structures (TLS), which are strongly associated with favorable prognosis in various cancers, span only $\sim 50,000\mu m^2$ (roughly $\sim 2,000$ pixels at $2\times$ magnification). However, analyzing their distribution requires considerably larger regions, approximately 1 cm^2 or up to 4 million pixels at the same magnification, due to tumor heterogeneity and the sparse nature of TLS [2, 39]. Moreover, WSIs encapsulate hierarchical information, with multi-scale contexts intricately intertwined. For tasks like diagnosing gastric signet ring cell carcinoma, both low- and high-magnification information are indispensable: large-scale regions at low magnification help detect potential tumor areas, while high-magnification is essential for examining cell morphology. Without effective integration of multi-scale information, errors such as misclassifying signet ring cells as foam or mucinous cells could lead to severe diagnostic errors¹.

Most existing WSI analysis methods follow a two-stage pipeline [4, 48]. First, WSIs are divided into small patches (e.g., 256×256 pixels), and a pre-trained encoder is used to extract features from patches. Second, these features are aggregated using methods such as multiple instance learning (MIL) to predict WSI-level outcomes. While this approach addresses the computational challenges of WSIs, it disrupts the flow of multi-scale information by isolating local and global features into separate stages. Consequently, hierarchical relationships across scales are lost during training, limiting the model’s capacity. A few recent efforts, such as LongViT [41], aim to maintain end-to-end training by optimizing Transformer memory usage. However, the massive number of tokens in gigapixel images, combined with their heavily pruned attention, hinder their performance.

To address these challenges, we propose Pixel-Mamba, a novel architecture designed for efficient and comprehensive WSI analysis. To tackle the computational burden, we leverage the Mamba module, a type of SSM with linear memory complexity, which has demonstrated exceptional performance in modeling ultra-long sequences [12, 54]. Furthermore, we argue that local inductive biases are particularly critical for WSI analysis. Small and spatially adjacent structures (e.g., cells) often combine to form meaningful larger structures (e.g., blood vessels), and similar local patterns can guide long-range dependencies. For instance, while TLS structures may be spatially distant, they are often morphologically similar. Pixel-Mamba integrates these insights by combining progressive token expansion

¹Using low magnification alone may lead to confusion with foam cell clusters in certain cases, whereas relying solely on high magnification may result in confusion with mucinous cells.

with the Mamba module. Starting from pixel-level tokens, our network progressively expands the token receptive field across layers, reaching regions as large as 32×32 . This design introduces local inductive biases, enabling the effective learning of hierarchical information, akin to convolutional neural networks, while the Mamba module further ensures that long-range dependencies are modeled at every level. It allows the network to integrate both local and global information hierarchically, addressing both computational and methodological challenges. Our experiments demonstrate the effectiveness of Pixel-Mamba across a variety of datasets and tasks. Notably, without requiring any pathology-specific pre-training, Pixel-Mamba matches or even exceeding the performance of leading foundation models (FM) pre-trained on millions of WSIs or WSI-text pairs. This underscores the potential of Pixel-Mamba as a powerful and efficient framework and a simple practical baseline for end-to-end WSI analysis. Our main contributions can be summarized as follows:

- We propose Pixel-Mamba, a high-memory efficiency architecture designed for end-to-end WSI analysis.
- Pixel-Mamba introduces progressive tokens expansion to incorporate hierarchical local inductive biases, concurrently models long-range dependencies across all scales, and enables efficient modeling of gigapixel WSIs.
- Extensive experiments demonstrate that Pixel-Mamba achieves or surpasses the performance of SOTA FMs pre-trained on millions of WSIs or WSI-text pairs, without requiring any pathology-specific pre-training.

2. Related Work

2.1. Representation Learning in WSIs

Two-stage MIL: Existing MIL methods adopt a two-stage scheme. First, they divide WSIs into patches of fixed size using pre-processing tools like CLAM [26], and extract patch features using pre-trained feature extractors such as ResNet [14], ViT [1], or pre-trained foundation models [5, 27, 42, 48]. Most two-stage MIL methods focus on the second stage and aim to explore better strategies for aggregating patch-level representations into slide-level representations. With the success of Transformers [31, 32], the attention mechanism has been introduced to aggregate patch features. Attention-based MIL approaches aim to capture long-sequence relationships among tens of thousands patches through attention mechanisms, including ABMIL [19], TransMIL [36], ILRA-MIL [44], and others [22, 51, 53]. Due to the difficulties in capturing long-range dependencies, state space models have been used to model the relationships among patches by [11, 50].

Hierarchical Representation: Current methods usually only use the WSIs at $20\times$ magnification, while some works

take advantage of the multi-scale nature of WSIs. They can be roughly divided into two categories, depending on how to process the multi-scale information. Some works are parallel, for example, multi-resolution input [13, 37], multi-scale feature concatenation [22], and cross-resolution graph construction [15] are proposed to explore multi-scale representations simultaneously. Other works are cascaded: HIPT [3] and GigaPath [47] use different ViTs to encode tile-level and slide-level features stage by stage, where the output of the first stage is fed into the next stage. Similar works include those [6, 46].

End-to-end Methods: To optimize patch embedding for downstream tasks, ICMIL [40] attempts to fine-tune patch feature extractors in the MIL framework by establishing loss propagation from the classifier to the feature extractor through iterative training. However, the feature extractor and task head is not synchronously optimized. VPT-Surv [33] uses adaptors to transfer pre-trained models to WSI. LongViT [41] builds an end-to-end framework using LongNet [10], a vision Transformer with dilated attention that is pre-trained using 64 GPUs. Despite this, LongViT’s performance still lags behind two-stage MIL approaches with pre-trained foundation models and fails to capture hierarchical representations for WSIs. In this work, we aim to develop a lightweight and efficient end-to-end framework for WSI analysis.

2.2. Pathological Foundation Models

Most existing approaches for pathological analysis are based on the two-stage MIL framework, making the design and pre-training of the feature extractor crucial. Early methods [19, 26] employed the ResNet [14] or Swin Transformer [25] pre-trained on natural images like ImageNet as the feature extractor. To adapt these extractors to pathological images, other works have designed multiple pretext tasks [21, 49], contrastive learning strategies [17, 22], and generative modeling methods [28, 34] for pre-training. Recently, with the expansion of data scale and the development of multimodal learning, new pre-trained models, often referred to as foundation models (FMs), have been released. Typical FMs include CTransPath [42], PLIP [18], UNI [5], CONCH [27], GigaPath [48], and CHIEF [43]. Although these FMs can extract better patch embeddings for MIL, the limitations of the MIL framework and the fixed feature embeddings still constrain their performance.

2.3. Mamba in Computational Pathology

Compared with Transformer, state space models such as Mamba [8, 12] exhibit linear computational complexity for long sequence modeling and have been used as a new vision backbone, exemplified by [24, 54]. Recently, Mamba has been introduced into computational pathology

to model the long sequence relationships among image patches [11, 50] or as a patch extractor [29]. Although they have achieved certain performance improvements, they are still constrained by the limitations of the MIL framework. This paper leverages the linear computational complexity of Mamba and proposes a novel end-to-end framework for learning slide-level representations of pathological images.

3. Method

3.1. Framework

The Pixel-Mamba framework, illustrated in Figure 2, consists of three main steps: whole slide image serialization, the Pixel-Mamba network, and downstream task heads. To address the challenges associated with gigapixel WSIs, Pixel-Mamba begins by serializing each pixel of the WSI into tokens through a whole slide scan. The Pixel-Mamba network then processes these tokens layer by layer, progressively expanding their receptive fields to capture hierarchical information. At each level, it employs a state space model (SSM) to capture global context among tokens, ensuring that long-range dependencies are effectively modeled. Finally, Pixel-Mamba learns a slide-level representation of the WSI, which is passed through various output heads to perform downstream tasks such as image classification, tumor staging, and survival prediction. Thanks to the linear computational complexity of the SSM and the innovative design, which includes Token Expansion and Region Fusion, the framework supports end-to-end training with full-image WSI input, outperforming existing SOTA two-stage MIL solutions across multiple tasks.

3.2. Whole Slide Image Serialization

Given a whole slide image I of size $H \times W \times C$, Pixel-Mamba first tokenizes I into visual tokens $T = \{\tau_i, i \in [1, M]\}$, where H , W , and C represent image height, width, and channels, respectively. Here, τ_i denotes the i^{th} token, and M represents total number of visual tokens. Unlike previous approaches such as Vision Mamba [54] or Vision Transformer [1], which tokenize images into fixed-size patches (e.g., 16×16), Pixel-Mamba initially tokenizes each pixel individually, resulting in 1×1 pixel-wise tokens. As the tokens process through the Pixel-Mamba network, their receptive fields are progressively expanded, enabling the network to learn hierarchical representations. This is particularly important for capturing the multi-scale information inherent in pathological images.

Given the large height and width of WSIs, simple serialization strategies can cause neighboring tokens (e.g., tokens in upper and lower rows) to be far apart in the sequence, potentially disrupting the learning of inductive biases. To mitigate this issue, we employ a region-based zigzag scanning approach. As illustrated in Figure 2 (a), the image I

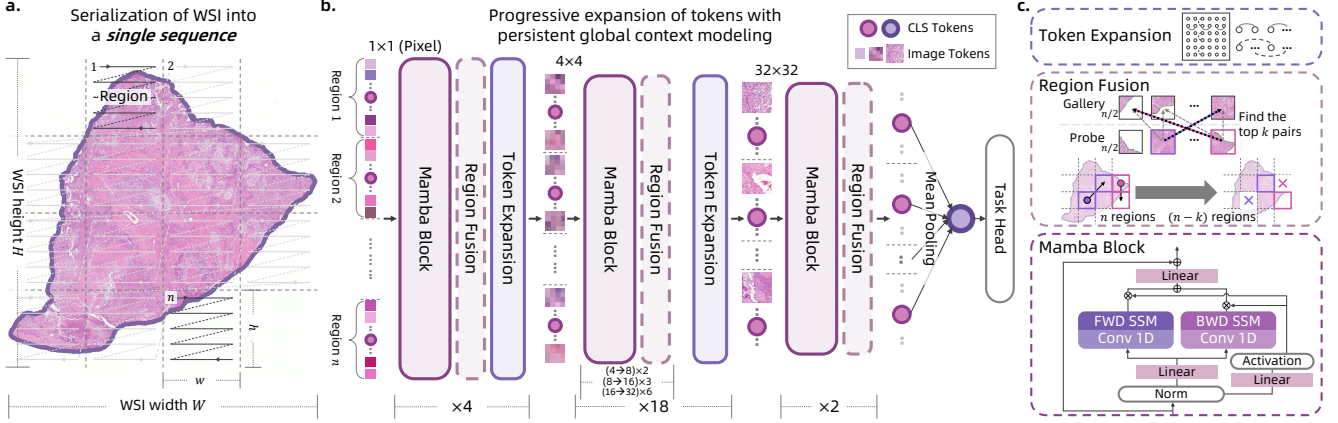


Figure 2. The Pixel-Mamba Framework. (a) The WSI is serialized, with CLS tokens added to create the token series T . (b) Pixel-Mamba progressively expands the receptive field of tokens while maintaining global context modeling. (c) Detailed illustrations of the Mamba Block, Region Fusion, and Token Expansion modules.

is divided into n regions of size $h \times w$, where h and w are the height and width of each region, respectively, and each region acts as a scanning window. Within each scan window, a zigzag scan is applied, and a CLS token is inserted at the center of the local sequence, resulting in a sequence length of $(h \times w + 1)$ for each region. The zigzag scan is then extended across all regions, ensuring the spatial proximity of neighboring tokens. Consequently, the total sequence length for the initial pixel-wise tokens of I is $M = H \times W + n$.

3.3. Pixel-Mamba Network

The architecture of the hierarchical network is shown in Figure 2 (b). The input to the network is the pixel-wise token series T generated by the whole slide image serialization. Each token τ initially has a size of $C = 3$, corresponding to the RGB channels. As the token receptive field expands during the forward process, the dimension C is progressively increased to accommodate richer representations. The network comprises $L = 24$ Pixel-Mamba layers, each consisting of three key components: Mamba Block, Region Fusion, and Token Expansion.

Throughout the forward process, the Mamba Block models global context among tokens to capture long-range dependencies. The Region Fusion module identifies similar regions at each level and merges them to reduce redundancy, improving memory efficiency. Finally, the Token Expansion module enlarges the token receptive field, progressively increasing it from 1×1 to 32×32 , which is crucial for learning hierarchical representations.

Mamba Block The architecture of the Mamba Block is shown at the bottom of Figure 2 (c). Following [54], Pixel-Mamba adopts the bi-directional SSM to model the long-range dependencies of tokens at each level. The forward

process within a Mamba Block is formulated as:

$$\begin{aligned}
 T^{l+1} &= fc(SSM_f(\psi(x)) \otimes z + SSM_b(\psi(x)) \otimes z) + T^l, \\
 x &= fc_x(norm(T^l)), \\
 z &= SiLU(fc_z(norm(T^l))),
 \end{aligned} \tag{1}$$

where T^l is the token series at the l^{th} layer of Pixel-Mamba, fc represents the linear layer, SSM_f and SSM_b denote the forward and backward branches of the bi-directional SSM, respectively, and ψ indicates the a Conv1D operation. The operator \otimes represents element-wise multiplication, while $SiLU$ is the SiLU activation function.

Region Fusion WSIs often contain hundreds of millions of pixels, posing significant computational challenges for model training. However, much of the information in them is redundant, offering opportunities to reduce complexity. To address this, Pixel-Mamba incorporates a Region Fusion module, which iteratively fuses similar regions layer by layer, reducing redundancy and computational overhead. The process is illustrated at the middle of Figure 2 (c). Given n regions with M tokens, the Region Fusion module partitions them into two equal sets: a gallery set and a probe set, each containing $n/2$ regions. For each region in the probe set, the cosine similarity $S^{ij} = \frac{CLS_g^i \cdot CLS_p^j}{\|CLS_g^i\| \cdot \|CLS_p^j\|}$, $i, j \in [1, n/2]$, is computed between the CLS token of this region and the CLS tokens of all regions in the gallery set, where CLS_g and CLS_p represent the CLS tokens from the gallery set and probe set, respectively.

The k region pairs with the highest similarity scores (Top- k) are then fused. Specifically, the k region pairs are merged by averaging the corresponding tokens from the token series of each paired region. The number of merged regions, k , is defined as $\lceil \alpha * n/L \rceil$, where $0 < \alpha < 1$ is a

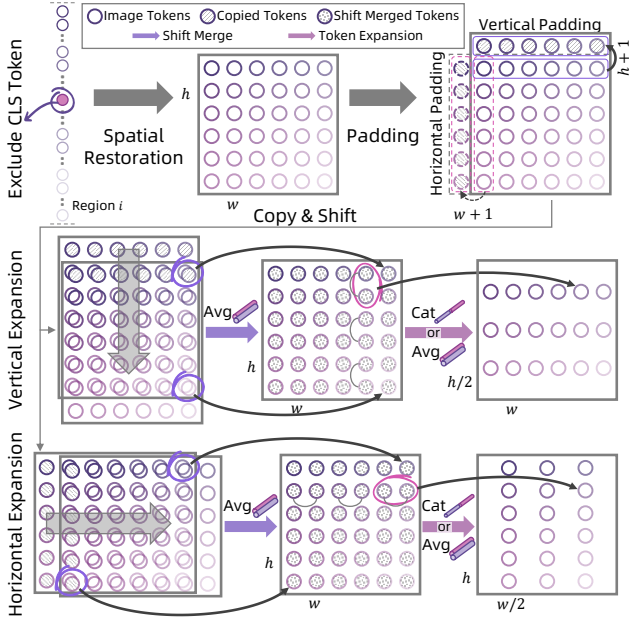


Figure 3. The illustration of Token Expansion in a region.

hyper-parameter controlling the retention rate of regions for the final output, and L is the total number of layers in the network. After fusion, the remaining number of regions is reduced to $n - k$.

Token Expansion Learning hierarchical token representations is critical for effective pathological image analysis. Pixel-Mamba employs a Token Expansion strategy to progressively enlarge the receptive field of tokens at key layers in the network. This enables the Mamba Block to capture multi-scale token representations at different levels.

The process of Token Expansion within a region is illustrated at the top of Figure 3. Token Expansion has two subtypes: vertical expansion and horizontal expansion, which are alternately applied across layers of the network. Given the token series of a region, the CLS token is first removed, and the remaining tokens are reshaped into an $h \times w \times C$ feature map. A shift merging operation is then applied, followed by token expansion. For vertical expansion, shift merging involves padding the first row, shifting the feature map down by one position, and averaging the shifted and original tokens to produce a new $h \times w \times C$ feature map with shift-merged tokens. The token expansion operation then increases the receptive field by concatenating or averaging adjacent tokens along the vertical dimension. The output size is $h/2 \times w \times 2C$ (if concatenating) or $h/2 \times w \times C$ (if averaging).

The horizontal Token Expansion follows a similar process but applies shift merging and token expansion along the w -dimension. The output size is $h \times w/2 \times 2C$ or

$h \times w/2 \times C$, depending on the operation (concatenating or averaging).

Token Expansion progressively enlarges the receptive field of tokens as the network deepens, enabling the Mamba Block to capture multi-scale representations across levels. This process allows Pixel-Mamba to extract hierarchical representations from WSIs. The final CLS tokens from merged regions are averaged into a single token for downstream tasks. Detailed network configurations are included in the supplementary material.

3.4. Task Heads

Both image classification and tumor staging are formulated as classification tasks by attaching a classification head, with cross-entropy loss used for training. For survival analysis, following the formulation in [52], the output CLS token from Pixel-Mamba is used to predict the hazard function $h(t)$, which is then used to compute the survival function $F(t)$. The negative log-likelihood loss \mathcal{L} is defined as:

$$\begin{aligned} \mathcal{L} = & - \sum_{(I,t,c) \in \mathcal{D}_{train}} c \cdot \log(F(t|I)) \\ & - \sum_{(I,t,c) \in \mathcal{D}_{train}} \{(1-c) \cdot \log(F(t-1|I)) \\ & + (1-c) \cdot \log(h(t|I))\}, \end{aligned} \quad (2)$$

where (I, t, c) represents the WSI, survival time, and right-censoring status of a patient in the dataset \mathcal{D} .

4. Experiments

4.1. Implemental Details

Implementation details for pre-training Pixel-Mamba on ImageNet and fine-tuning it on downstream datasets are provided in the supplementary materials.

Comparison: For the comparison on natural images, we evaluate Pixel-Mamba against other networks on the ImageNet-1K classification, including classical convolutional networks (**ConvNets**), Transformer architectures (**Transformers**), and current State Space Models (**SSMs**). The representative algorithms include ResNet [14], ViT [1], and Vim [54]. For the comparison on pathology images, we evaluate Pixel-Mamba against other methods on tumor staging and survival analysis. In computational pathology, most existing methods are based on a two-stage strategy of MIL, while Pixel-Mamba is an end-to-end method. Thus, we compare the **End-to-end** framework and **Two-stage** framework on all downstream tasks.

Two-stage: The two-stage framework typically consists of a feature extraction stage followed by an aggregation stage. In the first stage, many previous works employ different types of pre-trained image encoders, commonly referred to as pathological Foundation Models (FM). We select four

Table 1. Results of image classification on ImageNet-1K [9].

Method	Size	Params (M)	FLOPs (G)	Acc (%)
ResNet-18 [14]	224 ²	12	1.8	69.8
ResNet-50 [14]	224 ²	25	4.1	76.2
ResNet-101 [14]	224 ²	45	7.9	77.4
ResNet-152 [14]	224 ²	60	11.6	78.3
ResNeXt50 [45]	224 ²	25	4.3	77.6
ViT-B/16 [1]	384 ²	86	55.4	77.9
ViT-L/16 [1]	384 ²	307	190.7	76.5
DeiT-Ti [38]	224 ²	6	1.3	72.2
DeiT-S [38]	224 ²	22	4.6	79.8
S4ND-ViT-B [30]	224 ²	89	-	80.4
Vim-Ti [54]	224 ²	7.2	1.1	76.1
Vim-S [54]	224 ²	26	4.3	80.5
Pixel-Mamba-6M	224 ²	6.2	1.4	77.8
Pixel-Mamba-21M	224 ²	21	3.4	80.8

typical FMs: 1) **ResNet-50** [14] pre-trained on ImageNet, 2) Vision Foundation Model (**V-FM: GigaPath** [48]) pre-trained on 171K WSIs, 3) Vision Language Foundation Model (**VL-FM: CONCH** [27]) pre-trained on 1.17 million pathological image-caption pairs, and 4) ViT with hierarchical representation (**HIPT** [4], **Prov-GigaPath** [48]) pre-trained on 104M pathological image patches and 400K larger WSI regions. For the aggregation stage, we select five representative algorithms: MeanMIL, MaxMIL, AB-MIL [19], TransMIL [36], and ILRA-MIL [44]. These MIL methods are evaluated on the features extracted by the above FMs to compare the effects of different FMs.

End-to-end: To the best of our knowledge, only LongViT[41] has achieved end-to-end training on WSIs using a well-designed dilated attention network (LongNet)[10]. However, it requires 64 A100 GPUs for training, which is impractical for most researchers. We also compare LongViT with Pixel-Mamba across all downstream tasks.

4.2. Image Classification on Natural Images

Settings: We pre-train and evaluate Pixel-Mamba on natural images of ImageNet-1K [9], which includes more than 1.2 million images for training and 50k images for validation, covering 1000 different categories. Following previous works [38, 54], we use top-1 accuracy for evaluation.

Results: The results of image classification are summarized in Table 1. We pre-trained Pixel-Mamba in two configurations: Pixel-Mamba-6M and Pixel-Mamba-21M. Overall, compared to ConvNets, Transformers, and SSMs, Pixel-Mamba achieves the highest accuracies of 77.8% and 80.8% for the respective configurations. In particular, with an architecture similar to SSM, Pixel-Mamba-6M outperforms Vim-Ti by 1.7% in accuracy while using fewer model

parameters. These results demonstrate that Pixel-Mamba has a stronger capacity than other methods and lays a better pre-training foundation for downstream tasks.

4.3. Tumor Staging on Pathology Images

Settings: For tumor staging, we use Pixel-Mamba as the backbone network and add a linear layer as the staging head, which projects features into probabilities for four stages. This staging model is named Pixel-Mamba-Stage. Three datasets from The Cancer Genome Atlas (TCGA) are employed: Bladder Urothelial Carcinoma (BLCA), Breast Invasive Carcinoma (BRCA), and Lung Adenocarcinoma (LUAD). Each patient is classified into one of four tumor stages. Following previous work [23], due to the imbalanced number of patients in each stage, we use the macro-F1 score with 5-fold cross-validation for evaluation.

Results: The results of tumor staging are summarized in Table 2. Compared to different FMs such as ResNet-50, GigaViT, and CONCH, a better pre-trained FM significantly improves the performance of two-stage MIL approaches. Both vision FM (V-FM, GigaPath) and vision-language FM (VL-FM, CONCH) demonstrate comparable results. Overall, Pixel-Mamba-Stage outperforms two-stage MIL methods, two-stage hierarchical representation methods, and LongViT with macro F1 scores of 0.5334, 0.3744, and 0.3917 on the BLCA, BRCA, and LUAD datasets, respectively. Besides, all two-stage methods are pre-trained on large-scale pathological images or image-caption pairs, whereas LongViT is pre-trained on 10k WSIs. In contrast, Pixel-Mamba-Stage is only pre-trained on natural images, showcasing the efficacy of Pixel-Mamba.

4.4. Survival Analysis on Pathology Images

Settings: For survival analysis, we use Pixel-Mamba as the backbone network and add a linear layer as the survival head, which predicts the risk of patients, named Pixel-Mamba-Surv. The datasets used for survival analysis are BLCA, BRCA, and LUAD. Following previous work [4, 48], we use the Concordance index (C-index) with 5-fold cross-validation for evaluation.

Results: The results of survival analysis are summarized in Table 2. Similar to tumor staging, using pre-trained GigaPath and CONCH as feature extractors, two-stage MIL approaches achieve better results in C-index compared to using ResNet-50. Pixel-Mamba-Surv, pre-trained on only natural images, outperforms all two-stage MIL methods, two-stage hierarchical methods, and the end-to-end LongViT on the BLCA, BRCA, and LUAD datasets, with C-index values of 0.6507, 0.6707, and 0.6468, respectively. These results demonstrate that learning slide representations in an

Table 2. The results of the tumor staging and survival analysis on pathology images. V-FM: Vision Foundation Model. VL-FM: Vision-Language Foundation Model. The best results are highlighted in **bold**, and the second-best results are in underlined.

Tasks			Tumor Staging (5 Fold - Macro F1 Score)			Survival Analysis (5 Fold - C-index)		
Methods	Backbone	Params.	BLCA	BRCA	LUAD	BLCA	BRCA	LUAD
<i>Two-stage MIL; Patch features: ResNet-50 [14]; Pre-training: ImageNet</i>								
MeanMIL	ResNet-50	25M + 4.1K	0.3760 ± 0.0689	0.1860 ± 0.0049	0.1800 ± 0.0089	0.5256 ± 0.0564	0.5303 ± 0.0535	0.5883 ± 0.0803
MaxMIL		25M + 4.1K	0.3640 ± 0.0745	0.1840 ± 0.0049	0.1880 ± 0.0223	0.5250 ± 0.0548	0.5036 ± 0.0707	0.5009 ± 0.0703
ABMIL [19]		25M + 0.9M	0.4100 ± 0.0498	0.2300 ± 0.0245	0.2540 ± 0.0242	0.5813 ± 0.0349	0.6118 ± 0.0331	0.6130 ± 0.0270
TransMIL [36]		25M + 2.7M	0.4200 ± 0.0268	0.2900 ± 0.0126	0.3020 ± 0.0417	0.5610 ± 0.0223	0.5689 ± 0.0273	0.5973 ± 0.0338
ILRA-MIL [44]		25M + 3.7M	0.4460 ± 0.0441	0.2400 ± 0.0261	0.2540 ± 0.0432	0.5570 ± 0.0219	0.5998 ± 0.0333	0.5725 ± 0.0519
<i>Two-stage MIL; Patch features: V-FM (GigaPath) [48]; pre-training: 171K WSIs</i>								
MeanMIL	ViT-G	1.1G + 6.1K	0.4880 ± 0.0426	0.3160 ± 0.0287	0.3140 ± 0.0233	0.6052 ± 0.0575	0.6255 ± 0.0391	0.6004 ± 0.0506
MaxMIL		1.1G + 6.1K	0.4240 ± 0.0939	0.1940 ± 0.0233	0.2360 ± 0.0233	0.5798 ± 0.0290	0.5803 ± 0.0357	0.5263 ± 0.0552
ABMIL [19]		1.1G + 1.2M	0.5220 ± 0.0662	0.3520 ± 0.0286	0.3820 ± 0.0331	0.5990 ± 0.0698	0.6594 ± 0.0437	0.6083 ± 0.0461
TransMIL [36]		1.1G + 2.9M	0.4720 ± 0.0458	0.2980 ± 0.0133	0.3200 ± 0.0420	0.6141 ± 0.0549	0.6291 ± 0.0580	0.5770 ± 0.0741
ILRA-MIL [44]		1.1G + 4.2M	<u>0.5320 ± 0.0487</u>	0.3640 ± 0.0294	0.3880 ± 0.0643	0.6153 ± 0.0397	<u>0.6528 ± 0.0430</u>	0.6006 ± 0.0714
<i>Two-stage MIL; Patch features: VL-FM (CONCH) [27]; pre-training: 1.17 million pathology image-caption pairs</i>								
MeanMIL	ViT-B	86M + 2.1K	0.5160 ± 0.0427	0.3040 ± 0.0326	0.3260 ± 0.0459	0.5977 ± 0.0305	0.6451 ± 0.0637	0.6174 ± 0.0704
MaxMIL		86M + 2.1K	0.4660 ± 0.0408	0.1860 ± 0.0080	0.2460 ± 0.0388	0.5701 ± 0.0588	0.5483 ± 0.0742	0.5731 ± 0.0626
ABMIL [19]		86M + 0.7M	0.5260 ± 0.0753	0.3340 ± 0.0320	0.3840 ± 0.0700	0.6057 ± 0.0344	0.6444 ± 0.0770	0.6399 ± 0.0578
TransMIL [36]		86M + 2.4M	0.5180 ± 0.0312	<u>0.3700 ± 0.0940</u>	0.3500 ± 0.0253	<u>0.6404 ± 0.0253</u>	0.6380 ± 0.0379	0.5879 ± 0.0389
ILRA-MIL [44]		86M + 3.2M	0.5160 ± 0.0561	0.3380 ± 0.0264	<u>0.3880 ± 0.0271</u>	0.6030 ± 0.0363	0.6532 ± 0.0409	0.6218 ± 0.0881
<i>Two-Stage Hierarchical Representation; pre-training: 104M pathology patches + 400K WSI regions</i>								
HIPT [4]	HIPT-ViT-6	24M + 2.2M	0.4660 ± 0.0185	0.3240 ± 0.0287	0.3480 ± 0.0299	0.5731 ± 0.0331	0.6139 ± 0.0446	0.5895 ± 0.0478
Prov-GigaPath (CLS token) [48]	ViT-LongNet	1.2G + 6.1K	0.4820 ± 0.0466	0.3060 ± 0.0388	0.2940 ± 0.0224	0.5435 ± 0.0635	0.5697 ± 0.0964	0.6044 ± 0.0294
Prov-GigaPath (feature) [48]	ViT-LongNet	1.2G + 1.2M	0.5200 ± 0.0486	0.3300 ± 0.0219	0.3500 ± 0.0452	0.5954 ± 0.0311	0.6193 ± 0.0313	0.6210 ± 0.0724
<i>End-to-End; pre-training: ImageNet + 10K WSIs</i>								
LongViT [41] (0.6x)	ViT-S	22M	0.2310 ± 0.0731	0.3049 ± 0.0137	0.2757 ± 0.0240	0.5885 ± 0.0439	0.6453 ± 0.0699	0.5890 ± 0.0236
LongViT [41] (2.5x)	ViT-S	22M	0.4963 ± 0.0908	0.3068 ± 0.0276	0.3155 ± 0.0358	0.5789 ± 0.0506	0.6403 ± 0.0588	0.6085 ± 0.0140
LongViT [41] (5.0x)	ViT-S	22M	0.4757 ± 0.0847	0.2979 ± 0.0265	0.2809 ± 0.0196	0.5708 ± 0.0377	0.6316 ± 0.0832	0.6030 ± 0.0267
<i>End-to-End; pre-training: ImageNet</i>								
Pixel-Mamba-Stage/Surv (2.5x)	Pixel-Mamba	6.2M	0.5334 ± 0.0608	0.3744 ± 0.0163	0.3917 ± 0.0125	0.6507 ± 0.0485	0.6707 ± 0.0728	0.6468 ± 0.0331

end-to-end manner can surpass existing two-stage methods, even without pre-training on pathological images.

In addition, we analyze the performance of four different methods (ILRA-MIL, HIPT, LongViT, and Pixel-Mamba-Surv) using Kaplan-Meier analysis and the Log-Rank test to measure the statistical significance between low-risk and high-risk groups. The Kaplan-Meier curves after stratifying patients into low and high-risk categories based on their median predicted risk scores, are shown in Figure 4. Pixel-Mamba-Surv demonstrates better separation between the low-risk and high-risk groups compared to the other methods, and its lower p-value (0.0013) indicates statistically significant predictions.

4.5. Ablation Study

Two-stage vs End-to-end in WSIs: As shown in Table 2, although two-stage MIL approaches with pre-trained FMs achieve better results than end-to-end LongViT, end-to-end Pixel-Mamba-Stage/Surv without pre-training on pathological images outperforms both two-stage MIL approaches

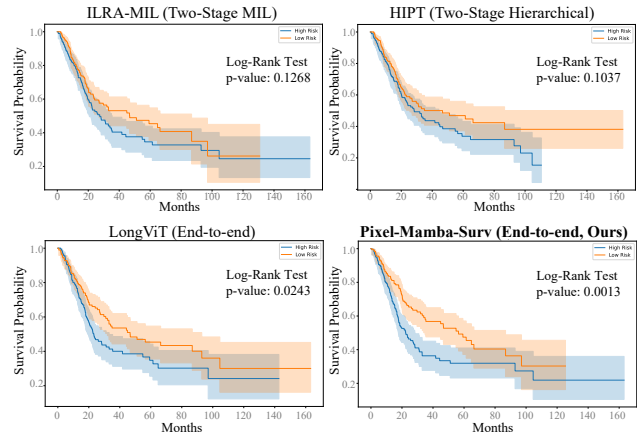


Figure 4. The comparison of Kaplan-Meier analysis and Log-Rank test (p-value, lower is best and p-value ≤ 0.01 indicates the statistical significance between two groups) on the BLCA dataset.

Table 3. Ablation study of end-to-end survival analysis on BLCA dataset. The used WSIs are at 2.5x magnification.

Method	Backbone	Params(M)	C-index
LongViT-Surv	ViT-S	22	0.5743 ± 0.0236
Vision-Mamba-Surv	Vim-Ti	7.2	0.5977 ± 0.0129
Pixel-Mamba-Surv	Pixel-Mamba	6.2	0.6507 ± 0.0485

Table 4. Ablation study of hierarchical tokenization on BLCA dataset. Hier-(1-32) indicates that the tokens of Pixel-Mamba are hierarchical, with token scales ranging from 1 to 32.

Method	Backbone	Token Scale	C-index
Vision-Mamba-Surv	Vim-Ti	16	0.5977 ± 0.0129
Vision-Mamba-Surv	Vim-Ti	32	0.5859 ± 0.0470
Vision-Mamba-Surv	Vim-Ti	16 + 32	0.6116 ± 0.0313
Pixel-Mamba-Surv	Pixel-Mamba	Hier-(1-32)	0.6507 ± 0.0485

and LongViT. To evaluate the end-to-end Pixel-Mamba, we transferred LongViT and Vision Mamba [54] into the survival prediction on the BLCA dataset. As shown in Table 3, Vision-Mamba-Surv outperforms LongViT-Surv by a relative 4.1% in C-index with fewer parameters. This demonstrates that the SSM-based long-sequence modeling scheme is more advantageous than the optimized dilated attention mechanism in LongViT when processing ultra-long tokens in WSIs. Furthermore, Pixel-Mamba-Surv with hierarchical slide representation outperforms Vision-Mamba-Surv by a relative 8.9% in C-index. This indicates that Pixel-Mamba, with its hierarchical representation and end-to-end optimization, is better at handling pathological images.

Hierarchical Tokenization: The token scales of existing two-stage methods or end-to-end LongViT are fixed (e.g., 16, 32), whereas hierarchical representation is crucial for WSI analysis. In Table 4, we present experiments using Vision-Mamba-Surv on two independent token scales: 16 and 32, achieving C-index values of 0.5977 and 0.5859, respectively. When combining the two tokens, Vision-Mamba-Surv achieves a higher C-index of 0.6116, indicating that multi-scale token representation is effective for WSI analysis. Moreover, utilizing hierarchical token representation with scales ranging from 1 to 32, Pixel-Mamba-Surv achieves a C-index of 0.6507. These results demonstrate that the proposed hierarchical representation is effective for pathological image analysis.

Scan Window of Pixel-Mamba: Pathological images often exceed 10,000 pixels in length and width, resulting in the initial number of Pixel-Mamba tokens surpassing 100 million. Directly applying the sequence scanning method of Vision Mamba would result in excessively long dis-

Table 5. Ablation study of scan window on BLCA dataset.

Method	Magnification	Scan window	C-index
Pixel-Mamba-Surv	2.5x	32	0.6083 ± 0.0562
Pixel-Mamba-Surv	2.5x	128	0.6190 ± 0.0374
Pixel-Mamba-Surv	2.5x	224	0.6507 ± 0.0485
Pixel-Mamba-Surv	2.5x	320	0.6242 ± 0.0386

Table 6. Ablation study of image scale on BLCA dataset.

Method	Backbone	Magnification	C-index
Pixel-Mamba-Surv	Pixel-Mamba	0.6x	0.5855 ± 0.0286
Pixel-Mamba-Surv	Pixel-Mamba	1.0x	0.6307 ± 0.0500
Pixel-Mamba-Surv	Pixel-Mamba	2.5x	0.6507 ± 0.0485

tances between spatially adjacent tokens. Inspired by Local Mamba [16], Pixel-Mamba introduces the scan window for processing pathological tokens, reducing the sequence distance between spatially adjacent tokens and enhancing the learning of local inductive biases. As shown in Table 5, Pixel-Mamba-Surv achieves the best results in the scan window size of 224×224 since it is pre-trained in this size.

Magnification of WSIs: Existing two-stage methods [5, 48] typically divide WSIs at 20x magnification into tens of thousands of tiles, capturing more fine-grained cellular details. Similar to LongViT [41], the end-to-end Pixel-Mamba can also adapt to images of various sizes. As shown in Table 6, with increasing input size, Pixel-Mamba-Surv achieves better results, realizing a C-index of 0.6507 on the BLCA dataset. These results demonstrate its scalability with the increasing number of tokens. Limited by GPU memory, the current Pixel-Mamba supports end-to-end training for WSIs at 2.5x magnification. Achieving end-to-end training on larger sizes will be our future work.

Discussion: Pixel-Mamba showcases the significant potential of hierarchical representation and end-to-end optimization in WSI analysis. Pixel-Mamba’s lightweight design, even without pre-training on pathology data, surpasses existing foundation models across multiple downstream tasks. This study emphasizes the importance of slide representation and end-to-end optimization. Future directions for Pixel-Mamba include: 1) gathering a sufficient number of WSIs for the pre-training of slide representation, and 2) optimizing the model structure to enable end-to-end training on 10x/20x magnified images to capture fine-grained details.

5. Conclusion

In this paper, we propose Pixel-Mamba, a novel end-to-end and practical framework with state space model (Mamba), for learning hierarchical slide representations of whole

slide image from pixels to gigapixels. Current multiple-instance learning methods rely heavily on the pre-training of foundation models with extensive histopathology data, while Pixel-Mamba achieves the results that surpass existing state-of-the-art multiple-instance learning methods in many downstream tasks, even without the pre-training on histopathology images. We believe that Pixel-Mamba offers a new and practical end-to-end optimization solution and can be a simple baseline for end-to-end histopathology image analysis, marking an important milestone in the advancement of histopathology image analysis by end-to-end whole slide representation learning.

A. Appendix

A.1. Network Configurations of Pixel-Mamba

The detailed network configurations of Pixel-Mamba-6M and Pixel-Mamba-21M are provided in Table 7 and Table 8, respectively.

Take Pixel-Mamba-6M for example, it consists of 24 Pixel-Mamba layers, each composed of three key components: Mamba Block, Region Fusion (RF), and Token Expansion (TE). Throughout the forward process, the Mamba Block models global context among tokens to capture long-range dependencies. The Region Fusion module identifies similar regions at each level and merges them to reduce redundancy, improving memory efficiency. Finally, the Token Expansion module enlarges the token receptive field, progressively increasing it from 1×1 to 32×32 , which is crucial for learning hierarchical representations. With the expansion of the token receptive field, the feature channels of tokens are increasing from 3 to 384. Pixel-Mamba includes horizontal TE and vertical TE. In each one, the token expansion operation then increases the receptive field by concatenating or averaging adjacent tokens along the horizontal or vertical dimensions.

Pixel-Mamba-21M also consists of 24 Pixel-Mamba layers. The difference is that its token feature channel increases to 768 throughout the forward process.

A.2. Implemental Details

Pre-training: Pixel-Mamba is pre-trained on the ImageNet [9] to ensure model convergence, utilizing over 1.28 million natural images for a classification task encompassing 1,000 categories. Following [54], Pixel-Mamba is trained on images of size 224×224 . The optimizer is AdamW with a momentum of 0.9, batch size of 1024, and weight decay of 0.05. Pixel-Mamba is trained for 300 epochs using a cosine learning rate schedule, starting with an initial learning rate of 0.001. Data augmentation techniques include random cropping, random horizontal flipping, label-smoothing regularization, mixup, and random erasing. 8 Nvidia A100 GPUs are used for pre-training,

Table 7. The detailed network configurations of Pixel-Mamba-6M. In the column of Pixel-Mamba Layers, Mamba represents the Mamba Block, RF represents the Region Fusion, and TE represents Token Expansion. The Token column indicates the receptive field of tokens in this layer.

Pixel-Mamba-6M			
Layer id	Token	Channels	Pixel-Mamba Layers
1	1×1	3	Mamba + RF + Horizontal TE-Cat
2	1×2	6	Mamba + RF + Vertical TE-Cat
3	2×2	12	Mamba + RF + Horizontal TE-Cat
4	2×4	24	Mamba + RF + Vertical TE-Cat
5	4×4	48	Mamba + RF
6	4×4	48	Mamba + RF + Horizontal TE-Cat
7	4×8	96	Mamba + RF
8	4×8	96	Mamba + RF + Vertical TE-Cat
9	8×8	192	Mamba + RF
10	8×8	192	Mamba + RF
11	8×8	192	Mamba + RF + Horizontal TE-Avg
12	8×16	192	Mamba + RF
13	8×16	192	Mamba + RF
14	8×16	192	Mamba + RF + Vertical TE-Avg
15	16×16	192	Mamba + RF
16	16×16	192	Mamba + RF
17	16×16	192	Mamba + RF
18	16×16	192	Mamba + RF
19	16×16	192	Mamba + RF
20	16×16	192	Mamba + RF + Horizontal TE-Avg
21	16×32	192	Mamba + RF
22	16×32	192	Mamba + RF + Vertical TE-Cat
23	32×32	384	Mamba + RF
24	32×32	384	Mamba + RF

costing approximately 2 to 3 days.

Fine-tuning on Downstream Tasks: Pixel-Mamba serves as the backbone network for all downstream tasks involving pathology images, including tumor staging and survival analysis. During fine-tuning, a task-specific head is added to the backbone network, and the entire network is fine-tuned on WSIs at a $2.5 \times$ magnification over 100 epochs. The AdamW optimizer is employed alongside a cosine learning rate schedule, starting with an initial learning rate of 0.0004. 8 Nvidia A100 GPUs are used. In each iteration, one GPU is assigned to process one WSI. Gradient accumulation is performed every 8 iterations, resulting in an effective batch size of 64.

Table 8. The detailed network configurations of Pixel-Mamba-21M. In the column of Pixel-Mamba Layers, Mamba represents the Mamba Block, RF represents the Region Fusion, and TE represents Token Expansion. The Token column indicates the receptive field of tokens in this layer.

Pixel-Mamba-21M			
Layer id	Token	Channels	Pixel-Mamba Layers
1	1×1	3	Mamba + RF + Horizontal TE-Cat
2	1×2	6	Mamba + RF + Vertical TE-Cat
3	2×2	12	Mamba + RF + Horizontal TE-Cat
4	2×4	24	Mamba + RF + Vertical TE-Cat
5	4×4	48	Mamba + RF
6	4×4	48	Mamba + RF + Horizontal TE-Cat
7	4×8	96	Mamba + RF
8	4×8	96	Mamba + RF + Vertical TE-Cat
9	8×8	192	Mamba + RF
10	8×8	192	Mamba + RF
11	8×8	192	Mamba + RF + Horizontal TE-Cat
12	8×16	384	Mamba + RF
13	8×16	384	Mamba + RF
14	8×16	384	Mamba + RF + Vertical TE-Avg
15	16×16	384	Mamba + RF
16	16×16	384	Mamba + RF
17	16×16	384	Mamba + RF
18	16×16	384	Mamba + RF
19	16×16	384	Mamba + RF
20	16×16	384	Mamba + RF + Horizontal TE-Avg
21	16×32	384	Mamba + RF
22	16×32	384	Mamba + RF + Vertical TE-Cat
23	32×32	768	Mamba + RF
24	32×32	768	Mamba + RF

experiments in the main text of the manuscript are obtained with $\alpha = 0.8$.

Table 9. The ablation study of α in Region Fusion.

α	0.4	0.6	0.8	1.0
C-index	0.6176	0.6260	0.6507	0.6104

A.3. The ablation of Region Fusion

In the Region Fusion module of Pixel-Mamba, the number of merged regions, k , is defined as $\lceil \alpha * n/L \rceil$, where $0 < \alpha < 1$ is a hyper-parameter controlling the retention rate of regions for the final output, and L is the total number of layers in the network.

We conduct the ablation study of hyper-parameter α and the results are reported in Table 9. Pixel-Mamba-Surv achieves the best C-index of 0.6507 with the $\alpha = 0.8$ on the BLCA dataset. Thus, we suggest $\alpha = 0.8$, and all results of

References

- [1] Dosovitskiy Alexey. An image is worth 16x16 words: Transformers for image recognition at scale. *ICLR*, 2021. 2, 3, 5, 6
- [2] Panagiotis Barmoutis, Matthew Di Capite, Hamzeh Kayhanian, William Waddingham, Daniel C Alexander, Marnix Jansen, and Francois Ng Kee Kwong. Tertiary lymphoid structures (tls) identification and density assessment on h&e-stained digital slides of lung cancer. *Plos one*, 16(9): e0256907, 2021. 2
- [3] Richard J Chen, Chengkuan Chen, Yicong Li, Tiffany Y Chen, Andrew D Trister, Rahul G Krishnan, and Faisal Mahmood. Scaling vision transformers to gigapixel images via hierarchical self-supervised learning. In *CVPR*, pages 16144–16155, 2022. 3
- [4] Richard J Chen, Chengkuan Chen, Yicong Li, Tiffany Y Chen, Andrew D Trister, Rahul G Krishnan, and Faisal Mahmood. Scaling vision transformers to gigapixel images via hierarchical self-supervised learning. In *CVPR*, pages 16144–16155, 2022. 2, 6, 7
- [5] Richard J Chen, Tong Ding, Ming Y Lu, Drew FK Williamson, Guillaume Jaume, Bowen Chen, Andrew Zhang, Daniel Shao, Andrew H Song, Muhammad Shaban, et al. Towards a general-purpose foundation model for computational pathology. *Nature Medicine*, 2024. 2, 3, 8
- [6] Zhen Chen, Jun Zhang, Shuanlong Che, Junzhou Huang, Xiao Han, and Yixuan Yuan. Diagnose like a pathologist: Weakly-supervised pathologist-tree network for slide-level immunohistochemical scoring. In *AAAI*, pages 47–54, 2021. 3
- [7] Germán Corredor, Xiangxue Wang, Yu Zhou, Cheng Lu, Pingfu Fu, Konstantinos Syrigos, David L Rimm, Michael Yang, Eduardo Romero, Kurt A Schalper, et al. Spatial architecture and arrangement of tumor-infiltrating lymphocytes for predicting likelihood of recurrence in early-stage non–small cell lung cancer. *Clinical cancer research*, 25(5): 1526–1534, 2019. 1
- [8] Tri Dao and Albert Gu. Transformers are ssms: Generalized models and efficient algorithms through structured state space duality. *arXiv preprint arXiv:2405.21060*, 2024. 3
- [9] Jia Deng, Wei Dong, Richard Socher, Li-Jia Li, Kai Li, and Li Fei-Fei. Imagenet: A large-scale hierarchical image database. In *CVPR*, pages 248–255. Ieee, 2009. 6, 9
- [10] Jiayu Ding, Shuming Ma, Li Dong, Xingxing Zhang, Shaohan Huang, Wenhui Wang, Nanning Zheng, and Furu Wei. Longnet: Scaling transformers to 1,000,000,000 tokens. *arXiv preprint arXiv:2307.02486*, 2023. 3, 6
- [11] Leo Fillioux, Joseph Boyd, Maria Vakalopoulou, Paul-Henry Cournède, and Stergios Christodoulidis. Structured state space models for multiple instance learning in digital pathology. In *MICCAI*, pages 594–604. Springer, 2023. 2, 3
- [12] Albert Gu and Tri Dao. Mamba: Linear-time sequence modeling with selective state spaces. *arXiv preprint arXiv:2312.00752*, 2023. 2, 3
- [13] Noriaki Hashimoto, Daisuke Fukushima, Ryoichi Koga, Yusuke Takagi, Kaho Ko, Kei Kohno, Masato Nakaguro, Shigeo Nakamura, Hidekata Hontani, and Ichiro Takeuchi. Multi-scale domain-adversarial multiple-instance cnn for cancer subtype classification with unannotated histopathological images. In *CVPR*, pages 3852–3861, 2020. 3
- [14] Kaiming He, Xiangyu Zhang, Shaoqing Ren, and Jian Sun. Deep residual learning for image recognition. In *CVPR*, pages 770–778, 2016. 2, 3, 5, 6, 7
- [15] Wentai Hou, Lequan Yu, Chengxuan Lin, Helong Huang, Rongshan Yu, Jing Qin, and Liansheng Wang. H²-mil: exploring hierarchical representation with heterogeneous multiple instance learning for whole slide image analysis. In *AAAI*, pages 933–941, 2022. 3
- [16] Tao Huang, Xiaohuan Pei, Shan You, Fei Wang, Chen Qian, and Chang Xu. Localmamba: Visual state space model with windowed selective scan. *arXiv preprint arXiv:2403.09338*, 2024. 8
- [17] Ziwang Huang, Hua Chai, Ruoqi Wang, Haitao Wang, Yue-dong Yang, and Hejun Wu. Integration of patch features through self-supervised learning and transformer for survival analysis on whole slide images. In *MICCAI*, pages 561–570. Springer, 2021. 3
- [18] Zhi Huang, Federico Bianchi, Mert Yuksekogun, Thomas J Montine, and James Zou. A visual–language foundation model for pathology image analysis using medical twitter. *Nature Medicine*, 29(9):2307–2316, 2023. 3
- [19] Maximilian Ilse, Jakub Tomczak, and Max Welling. Attention-based deep multiple instance learning. In *ICML*, pages 2127–2136. PMLR, 2018. 2, 3, 6, 7
- [20] Guillaume Jaume, Paul Doucet, Andrew H Song, Ming Y Lu, Cristina Almagro-Pérez, Sophia J Wagner, Anurag J Vaidya, Richard J Chen, Drew FK Williamson, Ahrong Kim, et al. Hest-1k: A dataset for spatial transcriptomics and histology image analysis. *arXiv preprint arXiv:2406.16192*, 2024. 1
- [21] Navid Alemi Koohbanani, Balagopal Unnikrishnan, Syed Ali Khurram, Pavitra Krishnaswamy, and Nasir Rajpoot. Self-path: Self-supervision for classification of pathology images with limited annotations. *TMI*, 40(10): 2845–2856, 2021. 3
- [22] Bin Li, Yin Li, and Kevin W Eliceiri. Dual-stream multiple instance learning network for whole slide image classification with self-supervised contrastive learning. In *CVPR*, pages 14318–14328, 2021. 2, 3
- [23] Jiawen Li, Yuxuan Chen, Hongbo Chu, Qiehe Sun, Tian Guan, Anjia Han, and Yonghong He. Dynamic graph representation with knowledge-aware attention for histopathology whole slide image analysis. In *CVPR*, pages 11323–11332, 2024. 6
- [24] Yue Liu, Yunjie Tian, Yuzhong Zhao, Hongtian Yu, Lingxi Xie, Yaowei Wang, Qixiang Ye, and Yunfan Liu. Vmamba: Visual state space model. *arXiv preprint arXiv:2401.10166*, 2024. 3
- [25] Ze Liu, Yutong Lin, Yue Cao, Han Hu, Yixuan Wei, Zheng Zhang, Stephen Lin, and Baining Guo. Swin transformer: Hierarchical vision transformer using shifted windows. In *ICCV*, pages 10012–10022, 2021. 3
- [26] Ming Y Lu, Drew FK Williamson, Tiffany Y Chen, Richard J Chen, Matteo Barbieri, and Faisal Mahmood. Data-efficient

- and weakly supervised computational pathology on whole-slide images. *Nature Biomedical Engineering*, 5(6):555–570, 2021. 2, 3
- [27] Ming Y Lu, Bowen Chen, Drew FK Williamson, Richard J Chen, Ivy Liang, Tong Ding, Guillaume Jaume, Igor Odintsov, Long Phi Le, Georg Gerber, et al. A visual-language foundation model for computational pathology. *Nature Medicine*, 30(3):863–874, 2024. 2, 3, 6, 7
- [28] Yang Luo, Zhineng Chen, Shengtian Zhou, Kai Hu, and Xieping Gao. Self-distillation augmented masked autoencoders for histopathological image understanding. In *BIBM*, pages 1343–1349. IEEE, 2023. 3
- [29] Ali Nasiri-Sarvi, Vincent Quoc-Huy Trinh, Hassan Rivaz, and Mahdi S Hosseini. Vim4path: Self-supervised vision mamba for histopathology images. In *CVPR*, pages 6894–6903, 2024. 3
- [30] Eric Nguyen, Karan Goel, Albert Gu, Gordon Downs, Preey Shah, Tri Dao, Stephen Baccus, and Christopher Ré. S4nd: Modeling images and videos as multidimensional signals with state spaces. *NeurIPS*, 35:2846–2861, 2022. 6
- [31] Zhongwei Qiu, Qiansheng Yang, Jian Wang, and Dongmei Fu. Ivt: An end-to-end instance-guided video transformer for 3d pose estimation. In *ACM MM*, pages 6174–6182, 2022. 2
- [32] Zhongwei Qiu, Huan Yang, Jianlong Fu, Daochang Liu, Chang Xu, and Dongmei Fu. Learning degradation-robust spatiotemporal frequency-transformer for video super-resolution. *TPAMI*, 2023. 2
- [33] Zhongwei Qiu, Hanqing Chao, Wenbin Liu, Yixuan Shen, Le Lu, Ke Yan, Dakai Jin, Yun Bian, and Hui Jiang. End-to-end multi-source visual prompt tuning for survival analysis in whole slide images. *arXiv preprint arXiv:2409.03804*, 2024. 3
- [34] Hao Quan, Xingyu Li, Weixing Chen, Qun Bai, Mingchen Zou, Ruijie Yang, Tingting Zheng, Ruiqun Qi, Xinghua Gao, and Xiaoyu Cui. Global contrast-masked autoencoders are powerful pathological representation learners. *PR*, 156:110745, 2024. 3
- [35] Joel Saltz, Rajarsi Gupta, Le Hou, Tahsin Kurc, Pankaj Singh, Vu Nguyen, Dimitris Samaras, Kenneth R Shroyer, Tianhao Zhao, Rebecca Batiste, et al. Spatial organization and molecular correlation of tumor-infiltrating lymphocytes using deep learning on pathology images. *Cell reports*, 23(1):181–193, 2018. 1
- [36] Zhuchen Shao, Hao Bian, Yang Chen, Yifeng Wang, Jian Zhang, Xiangyang Ji, et al. Transmil: Transformer based correlated multiple instance learning for whole slide image classification. *NeurIPS*, 34:2136–2147, 2021. 2, 6, 7
- [37] Hiroki Tokunaga, Yuki Teramoto, Akihiko Yoshizawa, and Ryoma Bise. Adaptive weighting multi-field-of-view cnn for semantic segmentation in pathology. In *CVPR*, pages 12597–12606, 2019. 3
- [38] Hugo Touvron, Matthieu Cord, Matthijs Douze, Francisco Massa, Alexandre Sablayrolles, and Hervé Jégou. Training data-efficient image transformers & distillation through attention. In *ICML*, pages 10347–10357. PMLR, 2021. 6
- [39] Mart van Rijthoven, Simon Obahor, Fabio Pagliarulo, Maries van den Broek, Peter Schraml, Holger Moch, Jeroen van der Laak, Francesco Ciompi, and Karina Silina. Multi-resolution deep learning characterizes tertiary lymphoid structures and their prognostic relevance in solid tumors. *Communications Medicine*, 4(1):5, 2024. 2
- [40] Hongyi Wang, Luyang Luo, Fang Wang, Ruofeng Tong, Yen-Wei Chen, Hongjie Hu, Lanfen Lin, and Hao Chen. Rethinking multiple instance learning for whole slide image classification: A bag-level classifier is a good instance-level teacher. *TMI*, 2024. 3
- [41] Wenhui Wang, Shuming Ma, Hanwen Xu, Naoto Usuyama, Jiayu Ding, Hoifung Poon, and Furu Wei. When an image is worth 1,024 x 1,024 words: A case study in computational pathology. *arXiv preprint arXiv:2312.03558*, 2023. 2, 3, 6, 7, 8
- [42] Xiyue Wang, Sen Yang, Jun Zhang, Minghui Wang, Jing Zhang, Junzhou Huang, Wei Yang, and Xiao Han. Transpath: Transformer-based self-supervised learning for histopathological image classification. In *MICCAI*, pages 186–195. Springer, 2021. 2, 3
- [43] Xiyue Wang, Junhan Zhao, Eliana Marostica, Wei Yuan, Jietian Jin, Jiayu Zhang, Ruijiang Li, Hongping Tang, Kanran Wang, Yu Li, et al. A pathology foundation model for cancer diagnosis and prognosis prediction. *Nature*, pages 1–9, 2024. 3
- [44] Jinxi Xiang and Jun Zhang. Exploring low-rank property in multiple instance learning for whole slide image classification. In *ICLR*, 2023. 2, 6, 7
- [45] Saining Xie, Ross Girshick, Piotr Dollár, Zhuowen Tu, and Kaiming He. Aggregated residual transformations for deep neural networks. In *CVPR*, pages 1492–1500, 2017. 6
- [46] Conghao Xiong, Hao Chen, Joseph JY Sung, and Irwin King. Diagnose like a pathologist: Transformer-enabled hierarchical attention-guided multiple instance learning for whole slide image classification. *arXiv preprint arXiv:2301.08125*, 2023. 3
- [47] Hanwen Xu, Naoto Usuyama, Jaspreet Bagga, Sheng Zhang, Rajesh Rao, Tristan Naumann, Cliff Wong, Zelalem Gero, Javier González, Yu Gu, et al. A whole-slide foundation model for digital pathology from real-world data. *Nature*, pages 1–8, 2024. 3
- [48] Hanwen Xu, Naoto Usuyama, Jaspreet Bagga, Sheng Zhang, Rajesh Rao, Tristan Naumann, Cliff Wong, Zelalem Gero, Javier González, Yu Gu, et al. A whole-slide foundation model for digital pathology from real-world data. *Nature*, pages 1–8, 2024. 2, 3, 6, 7, 8
- [49] Pengshuai Yang, Zhiwei Hong, Xiaoxu Yin, Chengzhan Zhu, and Rui Jiang. Self-supervised visual representation learning for histopathological images. In *MICCAI*, pages 47–57. Springer, 2021. 3
- [50] Shu Yang, Yihui Wang, and Hao Chen. Mambamil: Enhancing long sequence modeling with sequence reordering in computational pathology. *arXiv preprint arXiv:2403.06800*, 2024. 2, 3
- [51] Jiawen Yao, Xinliang Zhu, Jitendra Jonnagaddala, Nicholas Hawkins, and Junzhou Huang. Whole slide images based cancer survival prediction using attention guided deep multiple instance learning networks. *MIA*, 65:101789, 2020. 2

- [52] Shekoufeh Gorgi Zadeh and Matthias Schmid. Bias in cross-entropy-based training of deep survival networks. *TPAMI*, 43(9):3126–3137, 2020. [5](#)
- [53] Hongrun Zhang, Yanda Meng, Yitian Zhao, Yihong Qiao, Xiaoyun Yang, Sarah E Coupland, and Yalin Zheng. Dtfdmil: Double-tier feature distillation multiple instance learning for histopathology whole slide image classification. In *CVPR*, pages 18802–18812, 2022. [2](#)
- [54] Lianghai Zhu, Bencheng Liao, Qian Zhang, Xinlong Wang, Wenyu Liu, and Xinggang Wang. Vision mamba: Efficient visual representation learning with bidirectional state space model. *arXiv preprint arXiv:2401.09417*, 2024. [2](#), [3](#), [4](#), [5](#), [6](#), [8](#), [9](#)